INTERNATIONAL JOURNAL OF
NUMERICAL ANALYSIS AND MODELING
Volume 2, Supp , Pages 183–196

3D PRESTACK DEPTH MIGRATION WITH FACTORIZATION FOUR-WAY SPLITTING SCHEME

WENSHENG ZHANG AND GUANQUAN ZHANG

Abstract. 3D prestack depth migration is an important and commonly used way to obtain the images of complex structures in seismic date processing. In this paper, 3D prestack depth migration with hybrid four-way splitting scheme is investigated. Wavefield extrapolation is based on the 3D acoustic one-way. The hybrid four-way splitting algorithm based on factorization is derived. Numerical calculations of 3D post-stack depth migration for an impulse and 3D prestack depth migration for SEG/EAEG benchmark model are implemented. The result of 3D post-stack depth migration show that the numerical anisotropic errors can be reduced effectively and the errors are small when the lateral velocity variations is small. Moreover, the 3D prestack depth migration for SEG/EAEG model both with two-way and four-way hybrid splitting scheme can yield its good images. The Message Passing Interface (MPI) programme is adopted on PC cluster as the large scale computation of 3D prestack depth migration. The parallel efficiency is high because of high parallel feature of 3D prestack depth migration. The methods presented in this paper can be applied in field data processing.

Key Words. 3D, acoustic wave equation, hybrid method, factorization, four-way splitting, MPI.

1. Introduction

3D prestack depth migration is an important tool for complex structure imaging. There are two kinds of imaging methods. One is the Kirchhoff integral method based on ray tracing. The other is the non-Kirchhoff integral method based on wavefield extrapolation. Kirchhoff integral method is a high-frequency approximation method, which has difficulties in imaging complex structures. However, it can adapt sources and receivers configuration easily and has the advantage of less computation cost. Therefore it is still the dominant method of 3D prestack migration in oil industry. Non-Kirchhoff integral method, such as the finite-difference method, the phase-shift method (Gazdag, 1978), the split-step Fourier (SSF) method (Stoffa et al., 1990) and the Fourier finite-difference (FFD) method (Ristow and Ruhül, 1995), do wavefield extrapolation with one-way wave equation. It can yield precise images even in the case of complex structures or large lateral velocity variations. The FFD method is one of the most typical hybrid method, which combines both advantages of the phase-shift method and the finite-difference method.
Prestack depth migration can be implemented in the common-shot domain or in the common-offset domain. The full 3D common-offset prestack depth migration still has more difficulties in application because of its huge computational cost.

Compared with the shot-profile migration, the synthesized-shot migration has less computation cost. The synthesized-shot migration, which is based on the wavefield synthesis, first stacks or synthesises shot-gather records and sources, then extrapolates the synthesized wavefield. Therefore, its computation cost is comparable with that of multi-poststack migration. As the principle of the synthesized-shot migration is the same with that of the shot-profile migration, their imaging precisions are comparable.

For 3D one-way wave equation, a direct solution with stable implicit finite-difference scheme may lead to a non tri-diagonal system, which is computationally expensive. In order to decrease computation cost, the alternatively directional implicit (ADI) scheme is usually used. However, the two-way ADI algorithm may cause the problem of numerical anisotropic errors, which reaches maximum at 45° and 135° directions. In order to eliminate these errors, several authors proposed the multi-way splitting methods (Ristow and Rühl 1994; Collino and Joly, 1995). Among the multi-way splitting methods, such as three-way, four-way and six-way splitting methods, the four-way method is preferred as its computational grid is the retangle or square grid and there is no need to transform wavefield onto the triangle or hexagonal grid which three-way or six-way splitting method requires. It is well known that the seismic data observed on the surface is usually on the regular retangle or square grid. In this paper, the four-way splitting method based on factorization is proposed. It contributes to solve the tri-diagonal system both along 0°, 90° and 45°, 135° two ways respectively. Thus the high computational efficiency can be expected. Numerical calculations of 3D post-stack depth migration for an impulse and 3D prestack depth migration for SEG/EAEG benchmark model are completed. The results of 3D post-stack depth migration show that the numerical anisotropic errors can be eliminated effectively and the errors are small when the lateral velocity variations are small. Moreover, the results of 3D prestack depth migration both with hybrid two-way and four-way splitting schemes can give good images of the geologically complex structures of the SEG/EAEG model.

2. Methodology

2.1. four-way splitting scheme. Consider 3D acoustic wave equation

$$\frac{1}{v^2(x,y,z)}\frac{\partial^2 p}{\partial t^2} = \frac{\partial^2 p}{\partial x^2} + \frac{\partial^2 P}{\partial y^2} + \frac{\partial^2 p}{\partial z^2}, \tag{1}$$

where $p(x,y,z;\omega)$ is the pressure wavefiled at position (x,y,z), $v(x,y,z)$ is the media velocity. It is well known that the one-way wave equations for downgoing wave and upcoming wave in the frequency-space domain are given by

$$\frac{\partial P}{\partial z} = \pm i\frac{\omega}{v}\sqrt{1+\frac{v^2}{\omega^2}\frac{\partial^2}{\partial x^2}+\frac{v^2}{\omega^2}\frac{\partial^2}{\partial y^2}}P, \tag{2}$$

where ω is the circular frequency, i is the imaginary unit. The plus sign before the square-root represents downgoing wave and the minus sign represents upcoming wave. $P(x,y,z,\omega)$ is the wavefield in the frequency domain. Denote the square-root with A, i.e.,

$$A = \frac{i\omega}{v}\sqrt{1+\frac{v^2}{\omega^2}(\frac{\partial^2}{\partial x^2}+\frac{\partial^2}{\partial y^2})}. \tag{3}$$

Introducing a reference velocity $v_0(z)$, then this exact square-root operator can be approximated as

$$A = A_1 + A_2 + A_3, \tag{4}$$

with A_1, A_2 and A_3 are

$$A_1 = \frac{i\omega}{v_0}\sqrt{1+\frac{v_0^2}{\omega^2}(\frac{\partial^2}{\partial x^2}+\frac{\partial^2}{\partial y^2})}, \quad A_2 = i\omega(\frac{1}{v}-\frac{1}{v_0}), \quad A_3 = \frac{a\frac{v}{\omega}(\frac{\partial^2}{\partial x^2}+\frac{\partial^2}{\partial y^2})}{1+b\frac{v^2}{\omega^2}(\frac{\partial^2}{\partial x^2}+\frac{\partial^2}{\partial y^2})}, \tag{5}$$

respectively, where $a = \frac{1}{2}(1-\frac{v_0}{v})$, $b = \frac{1}{4}(\frac{v_0}{v})^2 + \frac{v_0}{v} + 1$ (Ristow and Ruhl, 1995), or $a = 0.47824(1-\frac{v_0}{v})$, $b = 0.37637(1+\frac{v_0^2}{v^2})$ (Zhang W., et al., 1999). One notes that the ratio v_0/v represents how the lateral velocity varies. The small it is, the large the lateral velocity variations are. If $v_0/v = 1$, then there is no lateral velocity variations. With the above approximations, the formal solution of the equation (2) can be written as

$$P(x,y,z+\Delta z,\omega) \approx P(x,y,z,\omega)e^{\pm i(A_1+A_2+A_3)\Delta z}. \tag{6}$$

In the equation (6), A_1 is the phase-shit operator to be applied in the frequency-wavenumber domain, A_2 is the well-known first-order correction term of Stoffa et al. (1990), A_3 is the finite-difference correction operator. The operator A_1 can be solved in the frequency-wavenumber domain with the help of fast Fourier transform. After completing the wavefield extrapolation with A_1, transforme the data of the frequency-wavenumber domain into that of the frequency-space domain, and solve the operator A_2 as a correction of the phase-shift.

The operator A_3 is commonly solved by the alternatively directional implicit scheme. For downgoing wave, the one-way equation of wavefield extrapolation can be expressed as

$$\frac{\partial P}{\partial z} = i\frac{a\frac{v}{\omega}(\frac{\partial^2}{\partial x^2}+\frac{\partial^2}{\partial y^2})}{1+b\frac{v^2}{\omega^2}(\frac{\partial^2}{\partial x^2}+\frac{\partial^2}{\partial y^2})}P \tag{7}$$

The finite-difference equation of equation (7) can be written as

$$\begin{aligned}&[1+(\alpha_1-i\beta_1)\delta_x^2+(\alpha_2-i\beta_2)\delta_y^2]P_{ij}^{n+1}\\ &=[1+(\alpha_1+i\beta_1)\delta_x^2+(\alpha_2+i\beta_2)\delta_y^2]P_{ij}^{n},\end{aligned} \tag{8}$$

where P_{ij}^n is the wavefield of $P(i\Delta x, j\Delta y, n\Delta z, \omega)$ (the discreted index of ω is omitted), δ_x^2 and δ_y^2 are the second-order difference operators with respect to x and y respectively. The coefficients α_1, α_2, β_1 and β_2 are related with spatial sampling steps, coefficients a and b, and can be written as

$$\alpha_1 = \frac{a(v^2+v_0^2)}{\omega^2\Delta x^2}, \quad \alpha_2 = \frac{a(v^2+v_0^2)}{\omega^2\Delta y^2}, \quad \beta_1 = \frac{a(v^2+v_0^2)}{2\omega\Delta x^2}, \quad \beta_2 = \frac{a(v^2+v_0^2)}{2\omega^2\Delta y^2}. \tag{9}$$

Based on the operator splitting method, the following alternatively directional implicit scheme of equation (8) can be obtained

$$\begin{aligned}[1+(\alpha_1-i\beta_1)\delta_x^2]P_{ij}^{n+1/2} &= [1+(\alpha_1+i\beta_1)\delta_x^2]P_{ij}^{n},\\ [1+(\alpha_2-i\beta_2)\delta_y^2]P_{ij}^{n+1} &= [1+(\alpha_2+i\beta_2)\delta_y^2]P_{ij}^{n+1/2},\end{aligned} \tag{10}$$

where $P_{ij}^{n+1/2}$ is the intermediate wavefield. We note that the second-order difference operator in equation (10) can be factorized further. That is to say, the second-order difference operator can be expressed as a product of the first-order

backward difference operator and the first-order forward difference operator, so equation (10) can be decomposed into the following system

$$\begin{aligned}
(I-\alpha_l\delta_x^+)P_{i,j}^{n+\frac{1}{4}} &= (I-\alpha_r\delta_x^+)P_{i,j}^{n},\\
(I+\alpha_l\delta_x^-)P_{i,j}^{n+\frac{2}{4}} &= (I+\alpha_r\delta_x^-)P_{i,j}^{n+\frac{1}{4}},\\
(I-\beta_l\delta_y^+)P_{i,j}^{n+\frac{3}{4}} &= (I-\beta_r\delta_y^+)P_{i,j}^{n+\frac{2}{4}},\\
(I+\beta_l\delta_y^-)P_{i,j}^{n+1} &= (I+\beta_r\delta_y^-)P_{i,j}^{n+\frac{3}{4}},
\end{aligned} \tag{11}$$

where $P_{i,j}^{n+\frac{1}{4}}$, $P_{i,j}^{n+\frac{2}{4}}$, $P_{i,j}^{n+\frac{3}{4}}$ are the intermediate wavefield, α_l, α_r, β_l and β_r are given by

$$\begin{aligned}
\alpha_l &= \tfrac{-1+\sqrt{4(\alpha_1-i\beta_1)}}{2}, \quad \alpha_r = \tfrac{-1+\sqrt{4(\alpha_1+i\beta_1)}}{2},\\
\beta_l &= \tfrac{-1+\sqrt{4(\alpha_2-i\beta_2)}}{2}, \quad \beta_r = \tfrac{-1+\sqrt{4(\alpha_2+i\beta_2)}}{2}.
\end{aligned} \tag{12}$$

respectively. Here, δ_x^+ and δ_x^- are the first-order difference operators forward and backward respectively with respect to x, δ_y^+ and δ_y^- are the first-order difference operators forward and backward respectively with respect to y, for example,

$$\begin{aligned}
\delta_x^+P_{i,j}^n &= P_{i+1,j}^n - P_{i,j}^n, \quad \delta_x^-P_{i,j}^n = P_{i,j}^n - P_{i-1,j}^n,\\
\delta_y^+P_{i,j}^n &= P_{i,j+1}^n - P_{i,j}^n, \quad \delta_y^-P_{i,j}^n = P_{i,j}^n - P_{i,j-1}^n.
\end{aligned} \tag{13}$$

The system (10) or (11) is the traditional two-way splitting scheme. The four-way solving algorithm may also be derived further by adding another two directions, i.e., 45° and 135° directions. Suppose x_1 is the 45° azimuth and y_1 is the 135° azimuth, then the alternatively directional implicit scheme along 45° and 135° two directions can be written as

$$\begin{aligned}
[1+(\bar{\alpha_1}-i\bar{\beta_1})\delta x_1^2]P_{ij}^{n+1/2} &= [1+(\bar{\alpha_1}+i\bar{\beta_1})\delta x_1^2]P_{ij}^n,\\
[1+(\bar{\alpha_2}-i\bar{\beta_2})\delta y_1^2]P_{ij}^{n+1} &= [1+(\bar{\alpha_2}+i\bar{\beta_2})\delta y_1^2]P_{ij}^{n+1/2},
\end{aligned} \tag{14}$$

where $\delta_{x_1}^2$ and $\delta_{y_1}^2$ are the two-order differential operator along x_1 and y_1 directions respectively. Like before, the equation (14) can be approximately decomposed into a system in which only the first-order difference operator is used

$$\begin{aligned}
(I-\bar{\alpha_l}\delta_{x_1}^+)P_{i,j}^{n+\frac{1}{4}} &= (I-\bar{\alpha_r}\delta_{x_1}^+)P_{i,j}^{n},\\
(I+\bar{\alpha_l}\delta_{x_1}^-)P_{i,j}^{n+\frac{2}{4}} &= (I+\bar{\alpha_r}\delta_{x_1}^-)P_{i,j}^{n+\frac{1}{4}},\\
(I-\bar{\beta_l}\delta_{y_1}^+)P_{i,j}^{n+\frac{3}{4}} &= (I-\bar{\beta_r}\delta_{y_1}^+)P_{i,j}^{n+\frac{2}{4}},\\
(I+\bar{\beta_l}\delta_{y_1}^-)P_{i,j}^{n+1} &= (I+\bar{\beta_r}\delta_{y_1}^-)P_{i,j}^{n+\frac{3}{4}},
\end{aligned} \tag{14}$$

where $\bar{\alpha_l}$, $\bar{\alpha_r}$, $\bar{\beta_l}$ and $\bar{\beta_r}$ are given by

$$\begin{aligned}
\bar{\alpha_l} &= \tfrac{-1+\sqrt{4(\alpha_1-i\beta_1)}}{2}, \quad \bar{\alpha_r} = \tfrac{-1+\sqrt{4(\alpha_1+i\beta_1)}}{2},\\
\bar{\beta_l} &= \tfrac{-1+\sqrt{4(\alpha_2-i\beta_2)}}{2}, \quad \bar{\beta_r} = \tfrac{-1+\sqrt{4(\alpha_2+i\beta_2)}}{2},
\end{aligned} \tag{16}$$

respectively. Here, $\delta_{x_1}^+$ and $\delta_{x_1}^-$ are the one-order forward and backward difference operators with respect to x_1 respectively, and $\delta_{y_1}^+$ and $\delta_{y_1}^-$ are one-order forward and backward difference operators with respect to y_1 respectively, for example we have

$$\begin{aligned}
\delta_{x_1}^+P_{i,j}^n &= P_{i+1,j+1}^n - P_{i,j}^n, \quad \delta_{x_1}^-P_{i,j}^n = P_{i,j}^n - P_{i-1,j-1}^n,\\
\delta_{y_1}^+P_{i,j}^n &= P_{i-1,j+1}^n - P_{i,j}^n, \quad \delta_{y_1}^-P_{i,j}^n = P_{i,j}^n - P_{i+1,j-1}^n.
\end{aligned} \tag{17}$$

The systems (11) and (15) form the hybrid four-way factorizational splitting scheme. Both they can be solved by recursive and anti-recursive algorithm or other fast algorithm like Thomas algorithm.

2.2. Wavefield synthesis method. The ideal of wavefield synthesis was originally proposed by Rietveld (Rietveld et al., 1994). And its synthesis application for the SEG/EAEG model was given in abstract format by Zhang (Zhang W., 2004). Here, we outline the main steps of wavefield synthesis as follows. Suppose $S(x, y, z_0, \omega)$ is the source wavefield in the frequency domain at position (x, y, z_0), and $H(x, y, z_0, \omega)$ is the synthesized-operator in the frequency-space domain, which can be written as (Rietveld et al., 1994)

$$H(x, y, z_0, \omega) = (e^{i\omega pr_1}, e^{i\omega pr_2}, \cdots, e^{i\omega pr_n}) \tag{18}$$

in the frequency-space domain, where p is the ray parameter which describes the incidence angle of the planewave, $r_i(x_i, y_i, z_0)$ is the known spatial position, z_0 is the depth at which the wavefield synthesis carries out. Then the synthesized-source $S_{syn}(x, y, z_0, \omega)$ can be written as

$$S_{syn}(x, y, z_0, \omega) = S(x, y, z_0, \omega)H(x, y, z_0, \omega), \tag{19}$$

Usually, a plane surface, i.e., $z_0 = 0$ is chosen. However, this is not necessary, and there is no need that z_0 is either the depth of data acquisition surface or the constant (represents a plane surface). With the synthesized-operator, the synthesized-record $R_{syn}(x, y, z, \omega)$ corresponding to the synthesized-source can be expressed similarly, that is

$$R_{syn}(x, y, z_0; \omega) = R(x, y, z_0, \omega)H(x, y, z_0, \omega), \tag{20}$$

where $R(x, y, z_0, \omega)$ is the shot-gather data in the frequency domain corresponding to the source $S(x, y, z_0, \omega)$. Therefore, the synthesized-source $S_{syn}(x, y, z, \omega)$ and its corresponding synthesized-record $R_{syn}(x, y, z, \omega)$ can form a physical observation geometry. That is to say, the synthesized-source corresponds with the downgoing wavefield and the synthesized-record corresponds with the upcoming wavefield. It is noted that there is another wavefield synthesis named phase-encoding method proposed by Louis and Romero et al. (Louis and Romero et al., 2000). However, for 3D prestack depth migration, the synthesized-shot number is very limited when we keep good imaging quality (Zhang W., et al., 2002).

2.3. Imaging principle. The subsurface image can be obtained by extrapolating the downgoing wavefield $D(x, y, z, \omega)$ and upcoming wavefield $U(x, y, z, \omega)$ simultaneously, and then applying the imaging condition (Claerbout, 1985)

$$I(x, y, z) = \sum_{\omega} U(x, y, z, \omega)D(x, y, z, \omega)^* \tag{21}$$

at each image point, where $D(x, y, z, \omega)^*$ is the conjugate of the complex wavefield $D(x, y, z, \omega)$. Another imaging condition yielding the reflection coefficient can be written as

$$R(x, y, z) = \sum_{\omega} \frac{UD^*}{\varepsilon + DD^*}, \tag{22}$$

where $R(x, y, z)$ is the reflection coefficient varying with spatial positions. One notes that a small positive number ε is added to the denominator to keep stability of the quotient. However, this imaging condition probably produce noise which my destroy imaging quality. So the imaging condition (21) is preferred. The final

images are obtained by summing all the partial images. For the imaging condition of post-stack depth migration, the equation (21) is simplified as

$$I(x, y, z) = \sum_{\omega} U(x, y, z, \omega), \tag{23}$$

where $U(x, y, z, \omega)$ is the extrapolated upcoming wavefield.

3. Numerical calculations

3.1. 3D post-stack depth migration. 3D post-stack depth migration in the case of variable velocity for an impulse response is presented first. The grid number for x, y and z is 64, the spatial steps are all $15m$. The time step is $4ms$. We choose two types of velocity model. One represents the case of small lateral velocity variations with media velocity $v(x, y, z) = 3000 + 0.1x + 0.1y + 0.1z(m/s)$. The ratio of reference velocity $v_0(z)$ with media velocity $v(x, y, z)$ varies from 0.941 to 0.942. The other represents the case of large lateral velocity variations with media velocity $v(x, y, z) = 3000 + 2x + 2y + 2z(m/s)$. The ratio of reference velocity $v_0(z)$ with media velocity $v(x, y, z)$ varies from 0.442 to 0.564. The impulse of the known recorded date is Ricker wavelet with $20Hz$ main frequency located at the position of $(x, y, z, t) = (480m, 480m, 500ms)$. Figure 1 is the level or horizontal slices of the 3D post-stack depth migration result for the case of small lateral velocity variations. The sliced position is at the depth of $210m$. Figure 1(a) is the slice by the traditional two-way splitting scheme, figure 1(b) is that by the two-way splitting scheme but splitting along 45° and 135° two directions, and figure 1(c) is that by the four-way splitting scheme. Figure 2 are the $x - z$ vertical slices of 3D migration result at the position of $y = 360m$. And figure 2(a), figure 2(b) and figure 2(c) are the slices by the traditional two-way splitting, 45° and 135° diagonal two-way splitting and four-way splitting scheme respectively. Figure 3 is the level slices of 3D post-stack depth migration result for the case of large lateral velocity variations. The sliced position is at the depth of $360m$. Figure 3(a) is the slice by the traditional two-way splitting scheme, figure 3(b) is that by the two-way splitting scheme but splitting along 45° and 135° two directions, and figure 3(c) is that by the four-way splitting scheme. Figure 4 are the $x - z$ vertical slices of 3D migration result at the position of $y = 280m$. And figure 4(a), figure 4(b) and figure 4(c) are the slices by the traditional two-way splitting, 45° and 135° diagonal two-way splitting and four-way splitting scheme respectively. These results show that the numerical anisotropic errors of traditional two-way scheme are eliminated effectively as shown in figure 3. And that the numerical anisotropic errors is small for the media velocity with small lateral variations as shown in figure 1.

3.2. 3D prestack depth migration. 3D prestack depth migration for SEG/EAEG model with the hybrid method is completed. The SEG/EAEG model is a benchmark 3D complex model for testing the imaging abilities of 3D migration/inversion methods. The data set used in this test has 50 sources lines each with 96 shots. The line space is $160m$ and the shot space is $80m$. The steps of Δx, Δy and Δz are $40m$, $40m$ and $20m$ respectively. The record length is $4992s$ with $8ms$ time sampling. Let x is the inline direction and y the crossline direction. Figure 5 are the $y - z$ vertical slices of the velocity model and the 3D prestack depth migration result sliced at $x = 5100m$ along crossline direction. Figure 5(a) is the model slice, figure 5(b) is the slice of migration result yielded by the two-way splitting algorithm, and figure

5(c) is the slice of migration result yielded by the four-way splitting algorithm. Figure 6 are the $x-z$ vertical slices of the velocity model and the 3D prestack depth migration result sliced at $y = 6020m$ along crossline direction. Figure 6(a) is the model slice, figure 6(b) is the slice of migration result yielded by the two-way splitting algorithm, and figure 6(c) is the slice of migration result yielded by the four-way splitting algorithm. Figure 7 are the $x-y$ level slices of the velocity model and the 3D prestack depth migration result at $z = 4200m$. Figure 7(a) is the model slice, figure 7(b) is the slice of migration result yielded by the two-way splitting algorithm, and figure 7(c) is the slice of migration result yielded by the four-way splitting algorithm. These results show that the 3D prestack depth migration for SEG/EAEG benchmark model both with two-way and four-way splitting schemes can yield good images of the complex structures.

The computations of 3D prestack depth migration are completed with Message Passing Interface (MPI) parallel program on PC-cluster. The most efficient parallel programs are ones which attempt to minimize the communication between processors while still requiring each processor to accomplish basically the same amount of work. Ray parameter parallelism is adopted. In this parallelism, each processor solve the same problem but with different ray parameter. The main computations are the wavefield extrapolation for downgoing wave D and upgoing wave U and they can be accomplished independently. The images for each ray parameter can be obtained and final images are stacked together. So the computations have high parallel speedup ratio. The communications between processors are set at the begin of and the end of the computation. At the begin, the velocity model for migration is sent to its corresponding processor from the main node and then every processor does the same calculations. After images for each ray parameter is yielded, they are sent back to the main node and stack to produce the whole imaging results.

4. Conclusions

The hybrid four-way splitting schemes based on factorization are investigated. Numerical calculations both of the 3D post-stack depth migration for an impulse and 3D prestack depth migration for SEG/EAEG benchmark model are implemented. The results show that the numerical anisotropic errors can be reduced effectively by the four-way splitting scheme and the errors are small when the lateral velocity variations is small. Moreover, the 3D prestack depth migration for the SEG/EAEG model both with two-way and four-way hybrid splitting scheme can yield its good images. Generally, the two-way splitting hybrid method is preferred in order to save computation cost. In order to improve computational efficiency, the Message Passing Interface (MPI) programme is used in 3D prestack depth migration. The parallel efficiency is high because of high parallel feature of problem. The methods presented in this paper can be applied in field data processing.

5. Acknowledgements

This research is supported by the Major State Basic Research Program of Peoples's Republic of China (No. G1999032803) and the National Key Nature Science Foundation (No.40004003) and ICMSEC Institute Director Foundation. The computations are completed in the State Key Laboratory of Scientific/Engineering Computing (LSEC), Institute of Computational Mathematics and Scientific/Engineering

Computing (ICMSEC). The authors would like to thank prof. Sun Jiachang and Chen Peimin for their helps and supports for publishing this paper.

References

[1] Claerbout, F. F., 1985, Imaging of the Earth's Interior. Blackwell Scientific Publication.
[2] Gazdag, J., 1978, Wave equation migration with the phase-shift method: Geophysics, 73: 1342∼1351.
[3] Rietveld, W.E.A., Berkhout, A.J., 1994, Prestack depth migration by means of controlled illumination: Geophysics, 59(5), 801∼809.
[4] Ristow, D., and Ruhl, T., 1995, Fourier finite-difference migration: Geophysics, 59(12), 1882∼1893.
[5] Ristow, D. and Ruhl, T., 1997, 3-D implicit finite-difference migration by multiway splitting: Geophysics, 62:(2), 554∼567.
[6] Rickett, J., Claerbout, J. and Fomel, S., 1999, Implicit 3-D depth migration by wavefield extrapolation with helical boundary conditions: 68th SEG Meeting Expanded Abstracts, 1124∼1127.
[7] Stoffa, P. L., Forkema, J. T., de Luna Freire, R. M., et al., 1990, Split-step Fourier migration: Geophysics, 55(2), 410∼421.
[8] Zhang Wensheng, Zhang Guanquan, Hao Xianjun, 1999, Hybrid depth migration and its absorbing condition: Geophysical Prospecting Pectroleum (in Chinese), 38(3), 1∼7.
[9] Zhang Wensheng, Zhang Guanquan and Wu Fei, 2002, 3-D prestack depth migration with single-shot and synthesized-shot records: 72th SEG Meeting Expanded Abstracts, October 6-11, Salt Lake City, Utah, USA.
[10] Zhang Wensheng, 2004, 3D prestack depth migration with planewave synthesizing method: 74th SEG meeting Expanded Abstracts, 10-15 October, Denver, USA.

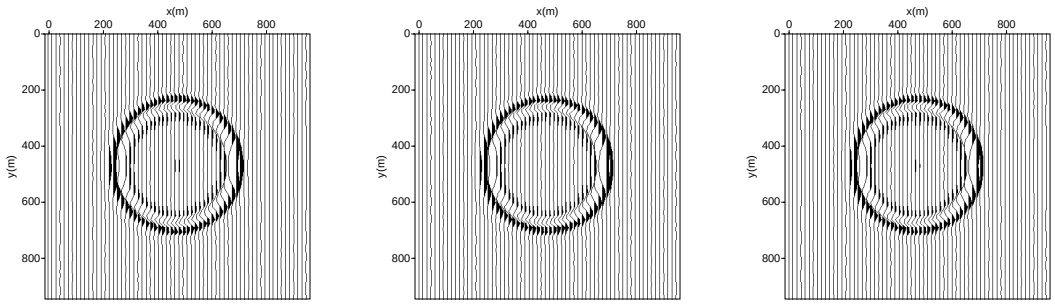

(a) (b) (c)

Figure 1. Horizontal slices of 3D post-stack depth migration for an impulse response with small lateral velocity variations. Hybrid wavefield extrapolation is used with (a) traditional two-way splitting, (b) 45° and 135° two-way splitting, (c) four-way splitting respectively.

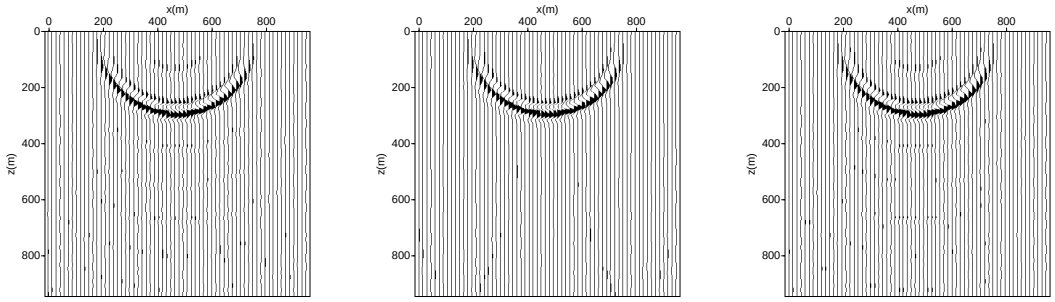

(a) (b) (c)

Figure 2. Vertical slices of 3D post-stack depth migration for an impulse response with small lateral velocity variations. Hybrid wavefield extrapolation is used with (a) traditional two-way splitting, (b) 45° and 135° two-way splitting, (c) four-way splitting respectively.

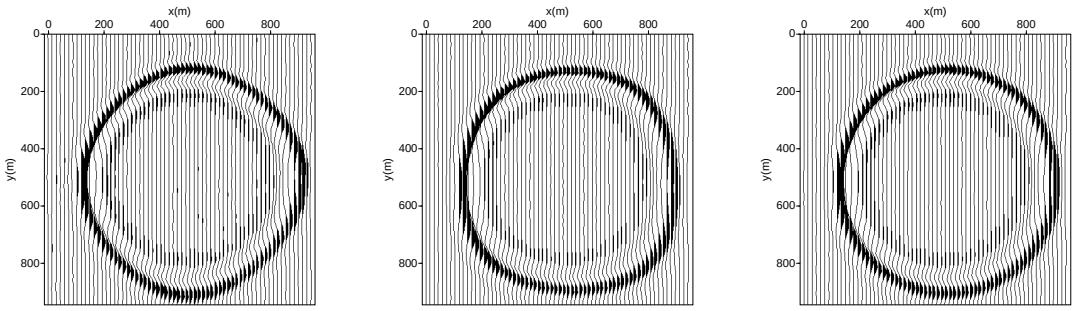

(a) (b) (c)

Figure 3. Horizontal slices of 3D post-stack depth migration result for an impulse response with large lateral velocity variations. Hybrid wavefield extrapolation is used with (a) traditional two-way splitting, (b) 45° and 135° two-way splitting, (c) four-way splitting respectively.

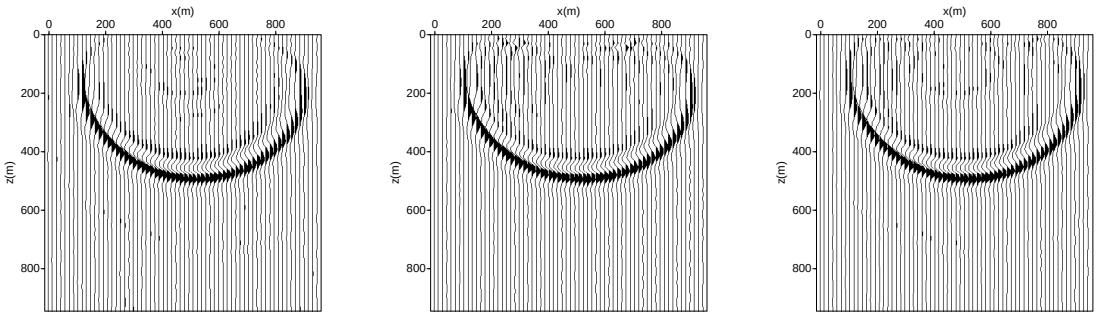

(a) (b) (c)

Figure 4. Vertical slices of 3D post-stack depth migration for an impulse response with large lateral velocity variations. Hybrid wavefield extrapolation is used with (a) traditional two-way splitting, (b) 45° and 135° two-way splitting, (c) four-way splitting respectively.

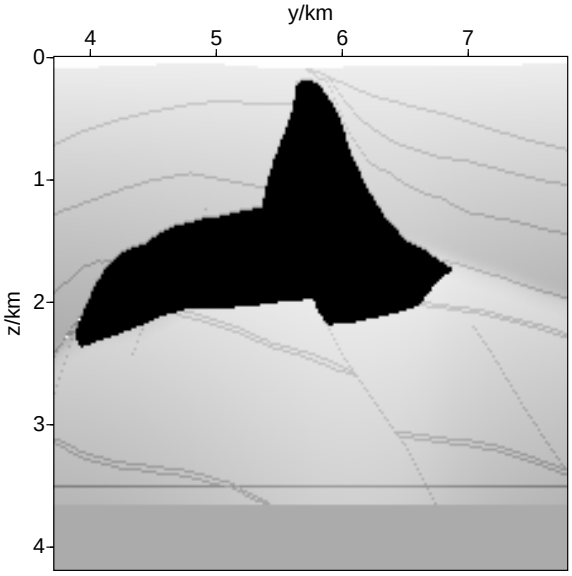

(a)

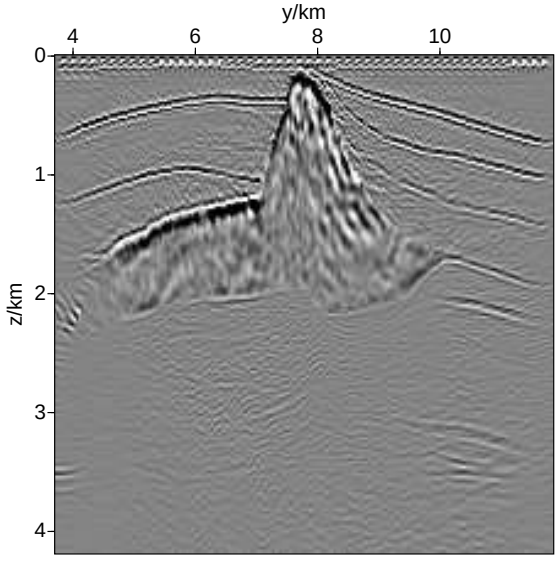

(b)

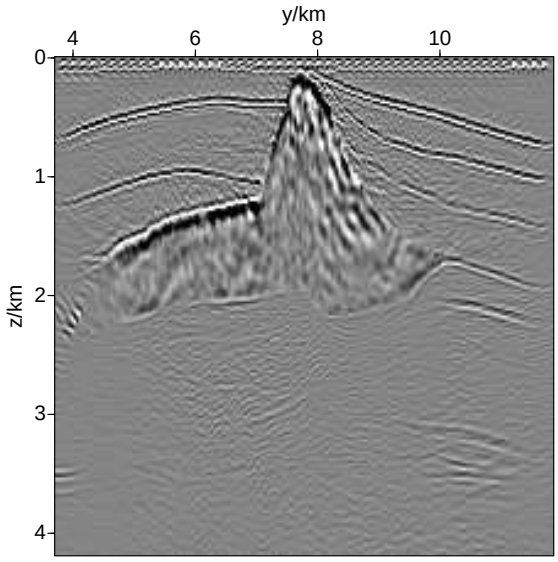

(c)

Figure 6. The $y-z$ vertical slices of velocity model and 3D prestack depth migration result sliced at the position of $x = 5100m$. (a) velocity model, (b) migration result yield by the two-way hybrid method, (c) migration result yield by the four-way hybrid method.

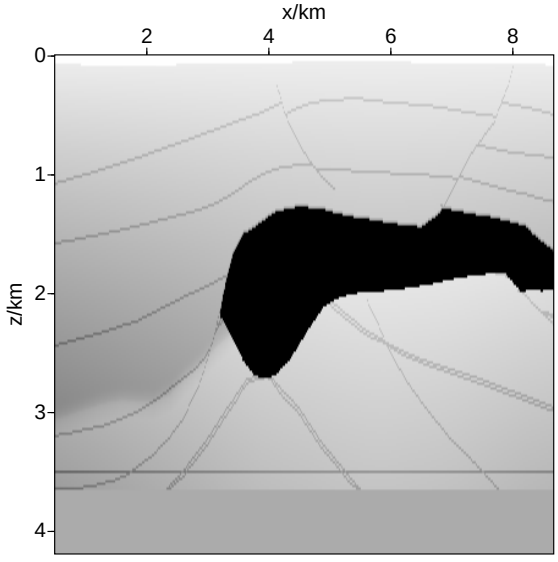

(a)

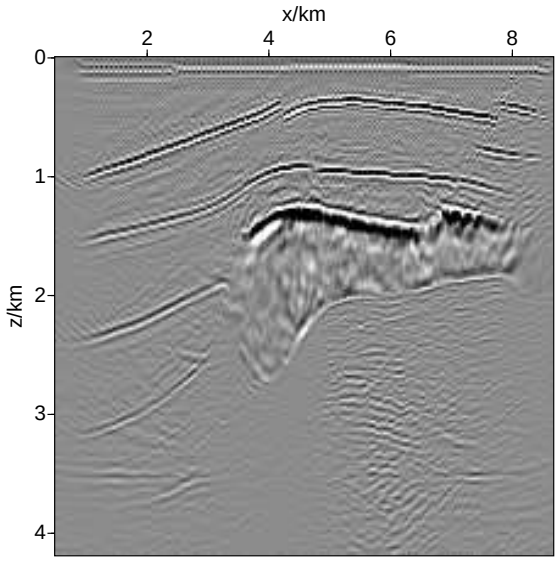

(b)

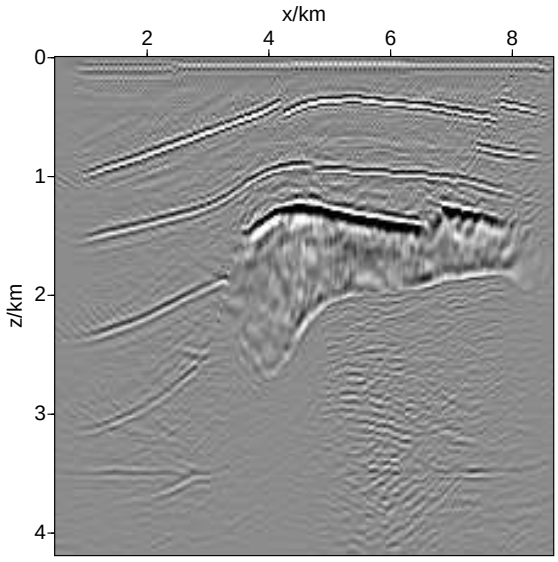

(c)

Figure 6. The $x-z$ vertical slices of velocity model and 3D prestack depth migration result sliced at the position of $y = 6020m$. (a) velocity model, (b) migration result yield by the two-way hybrid method, (c) migration result yield by the four-way hybrid method.

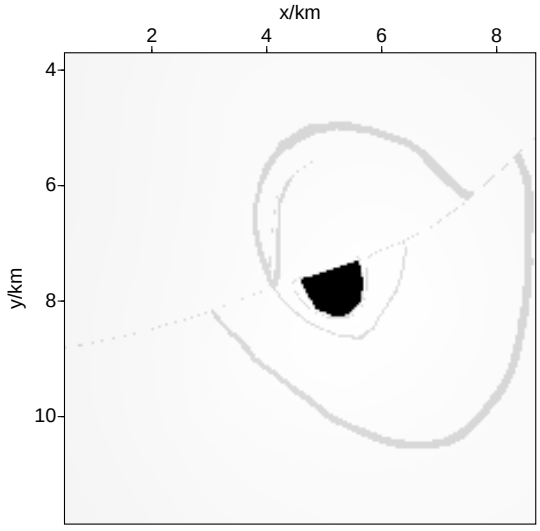

(a)

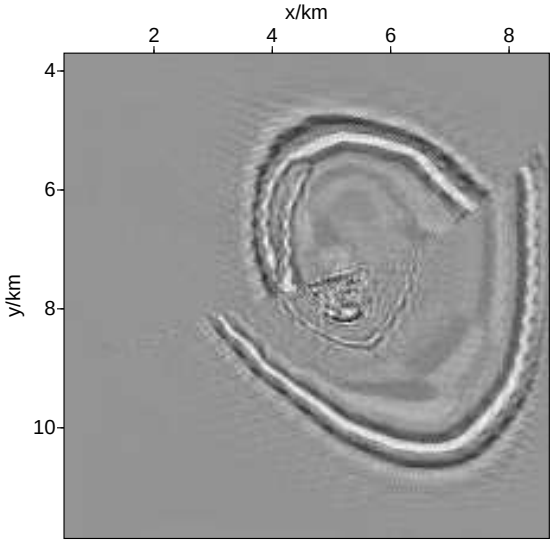

(b)

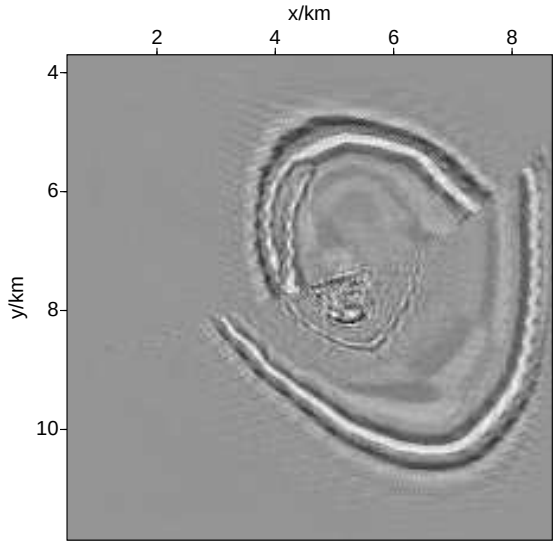

(c)

Figure 7. The $x-y$ level slices of velocity model and 3D prestack depth migration result sliced at the position of $z = 4200m$. (a) velocity model, (b) migration result yield by the two-way hybrid method, (c) migration result yield by the four-way hybrid method.

Institute of Computational Mathematics and Scientific/Engineering, Computing, LSEC, Academy of Mathematics and Systems Science, CAS, Beijing, 100080, China